Environmental Modelling & Software 58 (2014) 58–70

Contents lists available at ScienceDirect

Environmental Modelling & Software

journal homepage: www.elsevier.com/locate/envsoft

Distributed sediment yield modelling: Importance of initial sediment conditions

Gianbattista Bussi [a,*], Félix Francés [a], Juan José Montoya [a,1], Pierre Y. Julien [b]

[a] Research Institute of Water and Environmental Engineering, Universitat Politècnica de València, Camino de Vera s/n, 46022 Valencia, Spain
[b] Department of Civil Engineering, Colorado State University, Fort Collins, CO 80523-1372, USA

ARTICLE INFO

Article history:
Received 2 September 2013
Received in revised form
10 April 2014
Accepted 11 April 2014
Available online

Keywords:
Sediment modelling
Soil erosion
River network deposits
Initial conditions
Sediment hysteresis loop

ABSTRACT

The importance of initial sediment conditions on model calibration and validation is analysed. A sediment model was calibrated and validated under three different initial sediment conditions: (0) no sediment availability, (1) calibration of the initial sediment condition and (2) using a warm-up simulation. The model results were assessed in terms of the graphic of fine sediment transport, or sedigraphs, and the visual fit of the hysteresis on the sediment rating.

All strategies provided adequate results. However, the loop rating curve analysis demonstrated that the choice of initial sediment conditions affected the simulation results. Without any initial sediment condition, the model results were typically inferior to the simulation results with calibration or warm-up. The calibration of initial conditions proved to be the most reliable technique to generate clockwise hysteresis loops, but failed in reproducing other loop types. Overall, the warm-up simulations showed encouraging results, providing satisfactory fine sedigraph simulation results.

© 2014 Elsevier Ltd. All rights reserved.

1. Introduction

The integrated management of soil erosion and sediment redistribution at the catchment scale has acquired a great importance during the last decade (Owens and Collins, 2006). A common way to assess sediment production and transport is through a mathematical modelling approach (Harmon and Doe, 2001). Mathematical models are useful land management decision support tools. For example, sediment yield models are used to determine soil redistribution due to environmental changes (Van Rompaey et al., 2005).

There are many theoretical approaches to sediment modelling. A literature review can be found in Merritt et al. (2003), Aksoy and Kavvas (2005) and Karydas et al. (2012). All these studies point out that, during last decades, development of new models tended to produce conceptual and physically based distributed models. Some examples include EUROSEM (physically based mode, Morgan et al., 1998), LISEM (physically based model, de Roo et al., 1996), LASCAM (conceptual model, Viney and Sivapalan, 1999) or CatchMODS (conceptual model, Newham et al., 2004). This is because the sediment cycle is characterised by high complexity and non-linearity. These are features that simple empirical lumped models cannot describe easily. Moreover, the spatial variability of erosion and deposition processes is fundamental for catchment management decision support.

The last 60 years brought significant advances in sediment transport modelling but models are not without limitations (Favis-Mortlock et al., 2001). A strong limitation to the application of many existing sediment models is the need for a reliable calibration and validation (Jetten et al., 1999), which is required in order to prove the model robustness and reliability. In the past, modelling research studies highlighted the importance of calibration and validation for hydrological (Klemeš, 1986; Beven, 1989) and sediment models (de Roo and Jetten, 1999; Folly et al., 1999; Van Oost et al., 2005; Verstraeten, 2006; Polyakov et al., 2007). While hydrological model calibration is an issue that has been very often discussed in literature, very few papers describe clear and scientifically acceptable calibration and validation procedures for sediment models. Moreover, the use of automatic calibration algorithms in erosion and sediment yield modelling has been considered by Freedman et al. (1998) and Santos et al. (2003, 2010) for WESP model, Viney and Sivapalan (1999) for the LASCAM model and Ogden and Heilig (2001) for the CASC2D-SED model.

* Corresponding author. Present address: School of Geography and the Environment, University of Oxford, South Parks Road, OX1 3QY Oxford, UK. Tel.: +44 (0) 1865 285065.
E-mail address: gianbattista.bussi@ouce.ox.ac.uk (G. Bussi).
[1] Now at: Instituto de Hidrología, Meteorología y Estudios Ambientales (IDEAM), Carrera 10 No. 20-30, Bogotá, Colombia.

http://dx.doi.org/10.1016/j.envsoft.2014.04.010
1364-8152/© 2014 Elsevier Ltd. All rights reserved.

Relevant questions regarding sediment model calibration and validation include: (1) how to select the calibration and validation periods; (2) which objective function(s) is(are) to be used; and (3) which calibration technique is the most appropriate. One of the main problems is the estimation of the initial condition (defined as the initial value of model state variables). Typically, the most influent variables to be estimated at the beginning of a simulation are the antecedent soil moisture condition, the groundwater level, initial river flow stage and discharge and the initial in-channel sediment supply.

The initial sediment availability, i.e. the amount of sediment available for sediment transport at the beginning of the simulation. While the relevance of in-channel sediment deposits has already been highlighted by many authors, only a few papers analysed the influence of initial sediment availability on the sediment modelling process (e.g. Wicks and Bathurst, 1996). The mobilisation of sediment deposited by previous floods may cause a time gap between sediment concentration peak and water discharge peak, resulting in a clockwise hysteresis loop in the relationship between suspended sediment concentration and water discharge (or between sediment discharge and water discharge, i.e. the sediment rating curve). Several types of hysteresis loops are shown for example in Nistor and Church (2005). Hysteresis loop patterns can provide information about sediment erosion and transport interaction, rainfall intensity and duration, runoff production, sediment availability (e.g. Smith and Dragovich, 2009), etc. Different hysteresis loops depend on runoff and sediment transport processes and on the sediment source location(s) (e.g. Williams, 1989; Seeger et al., 2004; Eder et al., 2010). Particularly, clockwise hysteresis usually demonstrates that the catchment sediment dynamic is dominated by gully and river channel erosion rather than hillslope erosion (Piest et al., 1975; Nistor and Church, 2005). This situation is quite frequent: as many papers show, the relative contribution to total sediment yield of gully and river channel erosion and deposition might be very relevant compared to hillslope (or sheet and rill) erosion (Osterkamp and Toy, 1997; Merritt et al., 2003; de Vente et al., 2008; Smith and Dragovich, 2009; Vanmaercke et al., 2012).

Continuous simulation models also need an initial condition. In this case, while initial soil moisture and initial groundwater level can be estimated by simulating a relatively short warm-up period (Senarath et al., 2000; Brath et al., 2004), the available sediment strongly depends on the previous extreme events and a warm-up period length cannot be established *a priori*. Automatic calibration requires a high number of simulations and the processes involved in sediment yield modelling require a fine time discretisation. Therefore, due to computational time limitations, the calibration period must be as short as possible – although sufficiently long for an adequate calibration (Klemeš, 1986; Brath et al., 2004). Very often calibration is done using one or a few individual rainstorm events, thus increasing the influence of initial condition on model results.

In this study, different estimation techniques were investigated. Three sediment sub-models were calibrated and validated, employing different sediment initial condition estimation strategies: (0) no sediment availability, (1) manual calibration of the initial condition and (2) using warm-up simulation. Manual calibration and warm-up simulation are two common techniques for estimating initial sediment condition. The possibility of setting the initial sediment condition to zero (i.e. no available sediment in the drainage network) was also investigated in order to provide a reference to compare with the other two options.

In this study, the importance of initial sediment conditions on model calibration and validation was analysed using the model TETIS (Francés et al., 2002, 2007; Bussi et al., 2013). The TETIS model was modified, including some new features (automatic calibration algorithm, manual sediment initial condition setting tool and new calibration coefficients), in order to achieve the objectives of this study. It is a parsimonious model which takes advantage of all available spatial information. The TETIS model was selected especially for its flexible structure, which makes it suitable for a wide range of climatic and geological situations, and because it allows the automatic calibration of the hydrological and sediment parameters. In order to attain the objective of this study, the distributed hydrological and sediment model was applied and tested on the Goodwin Creek catchment (USA). The model results were assessed in terms of fine sedigraph (particle diameter less than 0.062 mm), hysteresis loop visual fit and several model metrics including the Nash and Sutcliffe Efficiency (NSE), the Root Mean Square Error (RMSE) and the Mean Absolute Error (MAE).

2. Model description

The TETIS model is based on two sub-models for the hydrology and sediment transport. Both sub-models are described as follows.

2.1. Hydrological sub-model

The TETIS hydrological sub-model is a distributed conceptual hydrological model developed for continuous simulation of the hydrological cycle. The model has been satisfactorily applied to different catchment areas (from less than 1 km^2 up to 60,000 km^2) at different spatial resolutions (square cells from 30 × 30 m to 500 × 500 m) under a wide range of climates (from semi-arid to humid). Some recent examples of these applications can be found in Francés et al. (2007, 2011), Vélez et al. (2009), Andrés-Doménech et al. (2010) and Salazar et al. (2013).

In TETIS each cell of the spatial grid describes the water cycle by means of five connected tanks. The relationships between tanks, representing the different hydrological processes, are described by simple linear reservoirs and flow threshold schemes. The processes described in the TETIS hydrological sub-model include snowmelt, canopy interception, soil capillary storage and evapotranspiration, overland runoff, soil gravitational storage and interflow, aquifer storage and base flow, and groundwater recharge. Overland runoff, interflow and base flow are connected to the stream network following the scheme represented in Fig. 1.The stream network is divided into gullies and river channels. Grid cells are classified, depending on their drainage area, into gully and river channel cells, by defining two drainage area thresholds. Every cell receives inflows from upstream and drains downstream following a 3D scheme generated from a Digital Elevation Model. Fig. 1 shows a 2D simplification of this scheme. Following the original classification from Francés et al. (2007), T2 refers to the superficial water storage

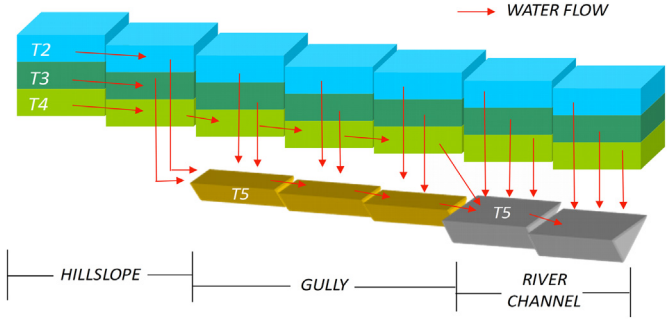

Fig. 1. Horizontal conceptual scheme of TETIS model for runoff propagation. T2 to T5 indicate the TETIS model tanks. In this figure, gullies and river channel threshold areas are equal to 2 and 5 cells, respectively.

tank, T3 to the topsoil water storage tank above field capacity, T4 to the aquifer storage tank and T5 to the gully or channel tank. The static storage tank T1 (not represented in Fig. 1) conceptualises the topsoil moisture below field capacity plus the interception and depression storage. The evapotranspiration is the only output from T1 and it plays an important role in determining the infiltration capacity at the beginning of storms. The overland flow and the interflow are routed respectively to the T2 and T3 tanks of the downstream cell; once both flows reach a cell whose drainage area is greater than the threshold drainage area corresponding to gullies, they move into T5 tank. In the same way, aquifer flow is routed to downstream T4 of cells until a second threshold drainage area (for river channels) is reached, and then it moves into T5 as base flow. Flow routing along the stream channel network is computed using the Geomorphologic Kinematic Wave methodology (Francés et al., 2007), which is based on a different parameterisation for gullies and for river channels.

The TETIS model includes an automatic calibration module, based on the SCE-UA optimisation algorithm (Shuffled Complex Evolution – University of Arizona, Duan et al., 1992, 1994). A wide range of objective functions are available to the user, including the Nash and Sutcliffe Efficiency coefficient (NSE – Nash and Sutcliffe, 1970), used in this study. The model effective parameters have a split structure, as presented by Francés et al. (2007). The calibration involves up to 9 correction factors (CFs), changing the specific parameter map as a whole, instead of correcting each value cell-by-cell, thus reducing drastically the number of variables to be calibrated.

2.2. Sediment sub-model

The TETIS sediment sub-model was presented in Bussi et al. (2013), although some new features were developed within this study. The TETIS sediment sub-model is coupled with the distributed hydrological conceptualisation and can be used both as event-based and continuous simulation model. Its structure is highly flexible and can be adapted to a wide range of climatic and geomorphologic conditions.

The TETIS sediment sub-model is based on the CASC2D-SED model, described in Johnson et al. (2000), Ogden and Heilig (2001) and Julien and Rojas (2002). Further model developments can also be found in England et al. (2007) and Velleux et al. (2006). Sediment production, transport and deposition are controlled by two factors: the sediment availability and the sediment transport capacity. Fine sediment transport is limited by the sediment availability on the catchment and this condition is termed supply-limited. Transport of coarse material is limited by flow transport capacity, also called capacity-limited (Julien, 2010a,b). The model separates sediment particles in textural classes (sand, silt and clay, following the US Department of Agriculture classification), assigning to each of them a representative grain diameter and settling velocity.

Hillslope soil erosion and sediment transport processes are described by means of the modified Kilinc and Richardson equation (Kilinc and Richardson, 1973; Julien, 2010a,b), which depends on discharge and terrain slope. The sediment volumetric discharge is computed as:

$$Q_h = \frac{1}{\gamma_s} W \alpha S_o^{1.66} \left(\frac{Q}{W}\right)^{2.035} \frac{K}{0.15} C P \quad \left(\mathrm{m^3\ s^{-1}}\right) \tag{1}$$

which is a function of the water discharge per unit width [Q ($\mathrm{m^3\ s^{-1}}$), cell overland discharge, divided by a representative width, W (m)]. In Eq. (1): S_o is the terrain slope ($\mathrm{m\ m^{-1}}$); γ_s is sediment specific weight (tons $\mathrm{m^{-3}}$); K, C and P are the Universal Soil Loss Equation (USLE) soil erodibility, cropping management and support practice factors respectively; and α is a dimensional and empirical parameter (around 25,000 for sandy bare soil with the expressed units).

The hillslope transport capacity calculated by Eq. (1) is divided into three parts, proportionally to the textural composition of the transported material (percentage of sand, silt and clay). Each transport capacity fraction is used to route the corresponding size fraction. These partial hillslope transport capacities are firstly used to route suspended sediments downstream (Fig. 2). Then, residual capacities are used to mobilise deposited material, and finally to erode the parent soil. The routed sediment is separated into suspended and deposited particles, depending on their settling velocity, as shown also in Fig. 2.

Gully and channel erosion and transport processes are computed through the Engelund and Hansen equation (Engelund and Hansen, 1967). Streamflow transport capacity depends on hydraulic radius, flow velocity, friction force and grain characteristics. The maximum sediment volumetric concentration is given by:

$$C_{w,i} = \beta \left(\frac{G}{G-1}\right) \frac{V S_f}{\sqrt{(G-1) g d_i}} \sqrt{\frac{R_h S_f}{(G-1) d_i}} \quad (-) \tag{2}$$

where: G is the sediment specific gravity (−); V is the flow velocity ($\mathrm{m\ s^{-1}}$); S_f is the energy slope (−); g is the gravitational acceleration ($\mathrm{m\ s^{-2}}$); d_i is the grain diameter of textural size class i (m); R_h is the hydraulic radius (m); and β is a nondimensional calibration coefficient (not existing in the original formulation). The streamflow transport capacity for the textural class i is expressed as follows:

$$Q_{s,i} = \frac{Q\ Cw_i}{\gamma_s} \quad \left(\mathrm{m^3\ s^{-1}}\right) \tag{3}$$

where Q is the stream (gully or river channel) discharge ($\mathrm{m^3/s}$). As for hillslopes, the streamflow transport capacity given by Eq. (3) for each textural class is firstly used to route sediment downstream and, if there is residual capacity, to mobilise deposited soil particles. The TETIS sediment sub-model does not consider parental material erosion in gullies and channels because the most important sediment source is the loose material deposited by previous floods (Piest et al., 1975).

To achieve the study objectives, the TETIS sediment sub-model was also coupled with an automatic calibration algorithm tool based on SCE-UA optimisation algorithm. This was done in order to automate the calibration procedure with a well-known calibration algorithm. Therefore, three sediment sub-model parameters can be calibrated: the α parameter in Eq. (1) for hillslope transport capacity, and two β coefficient from Eq. (2) (β_1 for gully transport capacity and β_2 for river channels transport capacity). These three variables are called sediment CFs, in the sense they are correcting Eqs. (1) and (2).

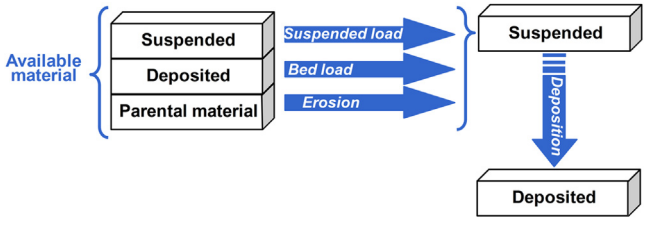

Fig. 2. Hillslope sediment process conceptualisation of TETIS model, after Rojas (2002).

Finally, a manual setting tool for the initial sediment condition was integrated into TETIS. The aim was to establish a given sediment volume of deposited material for each drainage network cell, including the possibility of choosing the material texture. Different volumes can be set for channel or gully cells.

3. Case study

The TETIS model was tested on the Goodwin Creek catchment. Goodwin Creek is a 21.3 km^2 experimental catchment situated in the Panola County (Mississippi, USA). The catchment is fully instrumented with 14 flow gauges and 32 rain gauges, in order to continuously monitor precipitation, runoff and sediment yield with a high spatial and temporal resolution. Fine sediment yield (particle diameter <0.062 mm) is monitored by discontinuous standard pumping samplers for fine solids. Sandy sediment yield is also measured manually using a DH-48 intake. Bedload is measured by means of a box sampler (Blackmarr, 1995). Since continuous series of total sediment load were not computed for every station (Kuhnle et al., 1989), only fine sediment series were used in this study.

Soils are mainly silt loams and the topography is quite smooth, with elevation ranging from 67 to 121 m a.s.l. Major land uses are pasture, agriculture and forest (44%, 13% and 27% respectively). The climate is humid, warm in summer and temperate in winter. The mean annual precipitation is 1440 mm, and convective rainfall events are common, especially in summer. The catchment hydrology is hortonian, with runoff almost entirely formed by overland flow, and an ephemeral base flow at the outlet. The catchment is affected by severe gullying, and many river stretches are deeply incised. Further information about Godwin Creek can be found in Blackmarr (1995), Alonso (1996), Kuhnle et al. (1996), Julien and Rojas (2002) and Kuhnle et al. (2005).

Precipitation, water discharge and fine sediment discharge continuous series from 1981 to 2008 are available. Five representative events, which occurred in August 1982, March 1983, May 1983, November 1983 and March 1984, were selected and used to calibrate and validate the TETIS model at the event scale. Their main characteristics are shown in Table 1. These events were recorded by 16 raingauges, and the corresponding water discharge and fine sediment discharge were available at 5 stream gauge stations (Q01, Q04, Q06, Q07, Q08), whose location are shown in Fig. 3. All data has a high and variable temporal resolution, but in order to use it as an input for the model, the hydrometeorological data were resampled with a 5 min temporal resolution.

Analysing the water discharge *vs* sediment discharge plots of all events and stations (sediment-rating curves), it was noticed that the most frequent hysteresis shape was the clockwise loop. A possible cause for this phenomenon has been attributed to variations in the local energy slope causing the stream velocity during the rising limb to be higher than during the falling limb at the same discharge (Boiten, 2003). This can also be attributed to an analysis of the terms of the Saint–Venant Equations for diffusive wave approximations (Julien, 2002). The observed clockwise hysteresis loop could also indicate that the catchment sediment dynamics is dominated by gully sediment mobilisation rather than upland erosion (Piest et al., 1975; Nistor and Church, 2005).

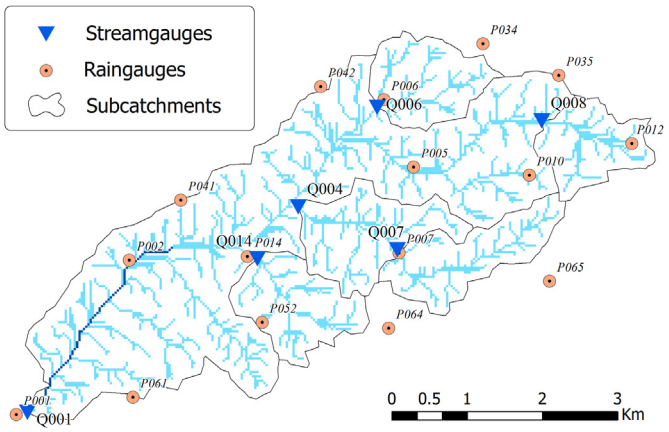

Fig. 3. Spatial distribution of raingauges and stream gauges within the Goodwin Creek catchment.

The information used for the estimation of the model parameters was taken from Blackmarr (1995). The Digital Elevation Model, resampled at 30 × 30 m, was used to derive flow direction, flow accumulation and slope maps. Maximum static storage (H_u) and saturated hydraulic conductivity (k_s) of the upper soil, shown in Fig. 4, were estimated using pedological information (texture, soil classification and soil profiles) and a proper pedotransfer function (Saxton and Rawls, 2006). The soil textural composition was also taken into account to estimate the *K* factor of the USLE, while vegetation cover, crop type and tillage method information were used to estimate the *C* USLE factor. Both maps are shown in Fig. 4. The *P* factor of the USLE was set to 1, since no support practice existed at the time of simulations. Textural maps are also a direct input of the model, since they define the grain size composition of eroded parent material from hillslopes.

In order to locate gully starting points, different drainage network maps were elaborated using different threshold areas, and these maps were subsequently compared to the real drainage network. The most likely map provided a gully threshold area of 0.01 km^2. The channel threshold area was obtained analysing at what point the permanent flow begins, providing an area of 15.3 km^2. Geomorphologic coefficients and exponents for Geomorphologic Kinematic Wave were taken from Molnár and Ramírez (1998).

4. Model calibration and validation

Given that soil erosion and sediment redistribution strongly depend on the hydrological cycle, Viney and Sivapalan (1999) proposed a two steps calibration procedure, which was adopted in this study: the hydrological sub-model is calibrated first, followed by the sediment sub-model.

Table 1
Main characteristics of the five storm events.

		Aug-1982	Mar-1983	May-1983	Nov-1983	Mar-1984
	Duration (hours)	8.5	25.4	14.1	8.3	9.9
	Mean areal accumulated rainfall (mm)	71	94	63	47	48
Water (at Q01)	Maximum discharge (m^3 s^{-1})	38	69	71	33	37
	Total volume (Hm^3)	0.407	1.177	0.746	0.324	0.354
Sediment (at Q01)	Maximum sediment discharge (m^3 s^{-1})	0.093	0.224	0.190	0.055	0.191
	Total volume (m^3)	597	1654	1337	306	1006

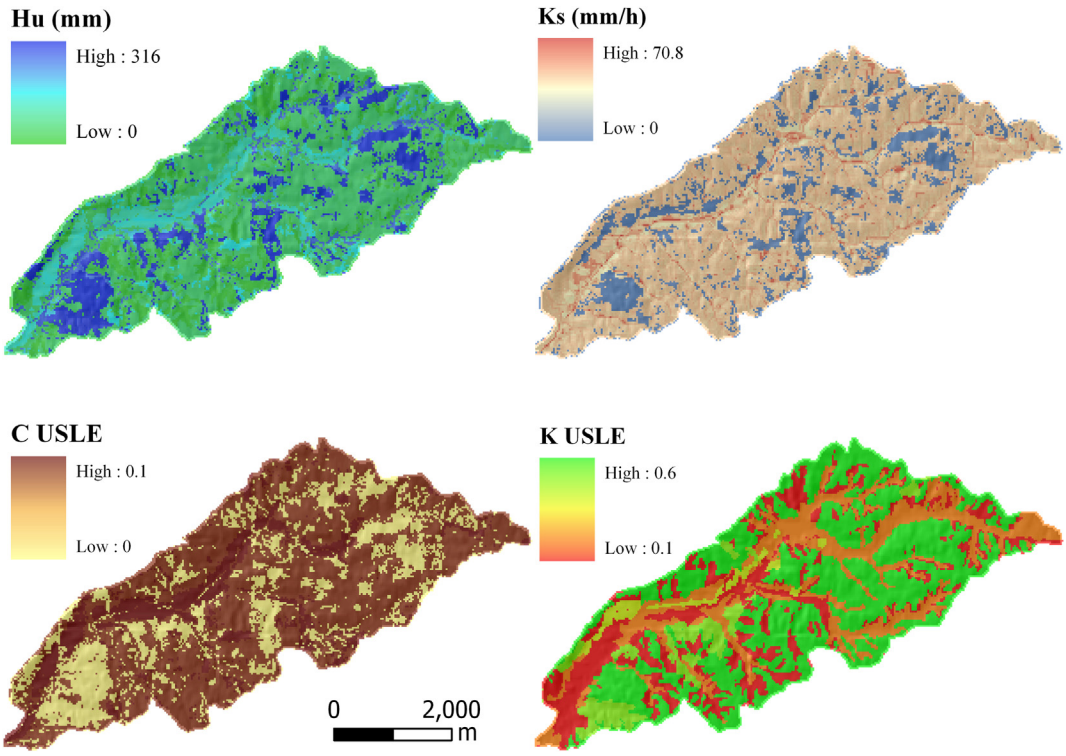

Fig. 4. Maps of the most influential hydrological and sediment spatial parameters of TETIS model in Goodwin Creek. Above: maximum static storage (H_u) and saturated hydraulic conductivity (k_s). Below: *C* and *K* factors of the Universal Soil Loss Equation.

4.1. Hydrological sub-model

The hydrological sub-model calibration was automatically carried out on the observed and simulated water discharges, using the SCE-UA algorithm with the NSE index as objective function. The calibration was performed at the catchment outlet (Q01) using the August 1982 event. The reliability of the calibrated model was further evaluated by checking that the hydrological predictions were satisfactory on different storm events and locations, a procedure often referred to as validation (Oreskes et al., 1994). The initial conditions of soil moisture, aquifer level and channel discharge were calibrated for all events. Fig. 5 shows the observed and simulated hydrographs of the calibration event and some representative validation events.

The resulting calibration NSE index was 0.97 (Q01, August 1982 event, Fig. 5a). The validation was carried out at the remaining stream gauges (Q04, Q06, Q07 and Q08) for the same event (spatial validation, Fig. 5b) and for the March 1983 event in all stream gauges (temporal and spatiotemporal validation, Fig. 5c and d respectively). Validation NSEs vary between 0.98 (May 1983 event, station Q01) and 0.61 (March 1984 event, station Q06), with a mean value of 0.83 and a median value of 0.86. The hydrological sub-model thus proved to perform very well, according to Moriasi et al. (2007). In fact it provides an accurate prediction of the stream flow across the catchment area. Moreover, the results provided by the TETIS model reproduced the observed hydrological behaviour of the catchment: the automatic calibrated runoff is almost entirely due to overland flow (99.6%), with a very small contribution from the interflow (0.4%) and a negligible contribution from base flow.

4.2. Sediment sub-model

Once the hydrological sub-model is validated, the sediment sub-model can be also calibrated and validated. The three sediment sub-model parameters can be calibrated separately, depending on the availability of stream records and position of stream gauges. The α and β_1 sediment sub-model parameters were automatically calibrated in a small sub-catchment without any river channel at the stream gauge station Q06 (Fig. 3). The β_2 parameter was also automatically calibrated but at the outlet (Q01), keeping the values of α and β_1 fixed.

The model was calibrated on a single event (1982) in order to emphasise the effect of sediment initial condition on the model calibration and validation. As for the hydrological sub-model, spatial and spatiotemporal validations were also carried out. In this case, the objective function considered to calibrate the simulated fine sediment discharges was the NSE index between calculated and observed fine sediment discharges. Moreover, a graphical goodness-of-fit on the sediment-rating curve between the observed and the simulated fine sediment vs water discharge (i.e.: the hysteresis loop) was used to discard calibration parameter sets giving acceptable NSE index values but not able to correctly reproduce the sediment dynamic of the catchment. The graphical goodness-of-fit was also used to analyse the effect of initial sediment condition.

The calibration and validation procedure of the sediment sub-model was repeated by varying the initial sediment condition while keeping the same hydrological conditions. First of all, the model was calibrated and validated without any initial sediment deposit, i.e. the initial condition of deposited sediment was set to 0. This was done in order to confirm the importance of in-channel sediment, as stated by many authors (e.g. Piest et al., 1975; Nistor and Church, 2005) and to prove that this model is able to take it into account.

Then, the initial sediment condition was estimated through two methodologies: *i)* calibration and *ii)* inclusion of a warm-up period. The calibration of the initial condition consisted of manually adjusting the initial amount of sediment deposited in the drainage

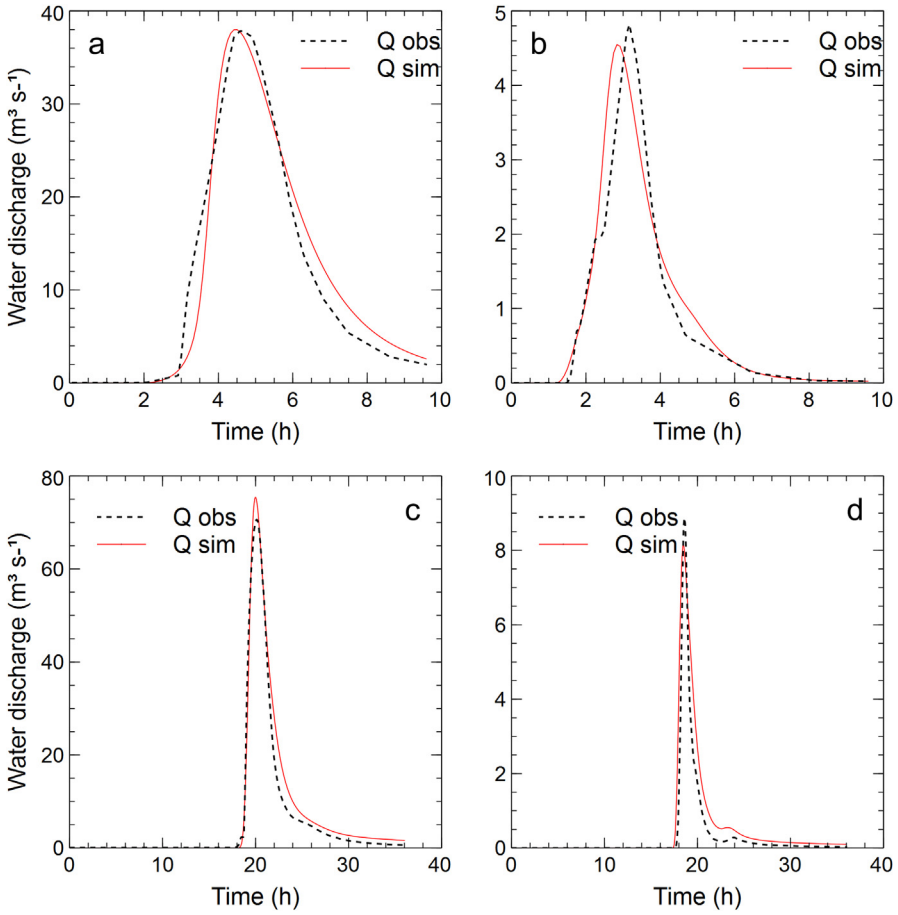

Fig. 5. TETIS model hydrological calibration and validation: (a) calibration in Q01, 1982 event; (b) spatial validation in Q06, 1982 event; (c) temporal validation in Q01, 1983 event; (d) spatiotemporal validation in Q06, 1983 event.

network (where the word "initial" means at the beginning of the event to be simulated). The warm-up period consisted of a warm-up simulation period preceding the event and was chosen to be long enough in such a way that longer warm-up periods would not affect the results.

5. Sediment sub-model results and discussion

For the sake of clarity, the different sediment initial condition strategies will be referred to as: no deposits (strategy 0); manual calibration (strategy 1); warm-up simulation (strategy 2). The results from the three strategies are shown in Table 2. The obtained correction factors for the three different strategies show some relevant differences, already suggesting that sediment initial condition strongly affects the TETIS model calibration.

From Table 2 it can be seen that strategy 0 provides higher α and β_1 coefficients (i.e. higher upstream transport capacity) than the other strategies. This is due to the strong influence of sediment initial condition on the model results. In fact, if no material is available for gully erosion at the beginning of the storm, the transport capacity must be higher in order to compensate for the supply-limited condition.

As expected, it was also noticed that the textural composition of deposited sediments strongly affected hysteresis loops. For this reason, in strategy 1 the sediment texture and volume deposited into the stream network were also calibrated. Table 3 shows the

Table 2
Sediment sub-model correction factors (α, β_1 and β_2) obtained by model calibration for three initial sediment condition strategies.

	Strategy		
	0	1	2
α	0.666	0.597	0.051
β_1	1.080	0.535	0.198
β_2	2.974	4.969	1.002

Table 3
Amount (m^3 m^{-1}) and texture of the calibrated initial sediment condition for strategy 1.

	Volume (m^3 m^{-1})	Sand (%)	Silt (%)	Clay (%)
Aug-1982				
Gullies	0.034	98	2	0
River channels	0.033	100	0	0
Mar-1983				
Gullies	0.042	78	22	0
River channels	0.033	100	0	0
May-1983				
Gullies	0.0035	96	3	1
River channels	0.085	39	59	2
Nov-1983				
Gullies	0.033	100	0	0
River channels	0.036	91	9	0
Mar-1984				
Gullies	0.050	67	33	0
River channels	0.033	100	0	0

sediment volume established as initial sediment condition for strategy 1. The material set as initial condition is rather coarse and the gully sediment is usually coarser than the channel sediment. This is due to the stream velocity, which is usually higher in gullies than river channels.

5.1. Model performance evaluation

Table 4 shows the sediment sub-model calibration and validation results in terms of NSE values, calculated on the observed/simulated fine sediment time series. Fig. 6 shows the fine sediment discharge for the five flood event at stations Q01 and Q06.

The median NSE values are 0.564, 0.598 and 0.572 for strategy 0, 1 and 2 respectively. The standard deviation of all NSE values is higher for strategy 1, due to some outlier values such as the ones obtained for events March 1983 and May 1983 in station Q06, and lower for strategy 0. The model validation performances were also assessed in terms of Root Mean Square Error (RMSE – Table 5), providing median values of 0.00231, 0.00236 and 0.00201 respectively, and in terms of Mean Absolute Error (MAE – Table 6), providing median values equal to 0.000436, 0.000591 and 0.000546 respectively. More information on these performance indexes can be found in Bennett et al. (2013). Strategy 0 provided the best results in terms of MAE, while strategy 1 provided the best results in terms of NSE and strategy 2 provided the best results in terms of RMSE, although all values are substantially similar. Both RMSE and NSE tend to assign more weight to larger events, though RMSE is more influenced by outliers. On the other hand, MAE reduces the bias towards highest peaks (Bennett et al., 2013). It can be stated that the performances of all strategies are satisfactory, comparable and almost equivalent. Furthermore, no dependency could be found between model strategy performance and event magnitude or duration. This means that no definitive conclusion can be pointed out regarding which strategy is more suitable than the other two for given flood event characteristics. This performance analysis can be supported by the visual fit shown in Fig. 6. The model performances of the three strategies for all events are very similar and there is no evidence that a strategy could perform much better than the others under some given event characteristics such as water or fine sediment discharge peak or volume. This can be considered somehow surprising, given that in strategy 0 the volume of the initial deposits was set to 0. This implies that, even if initial deposits are not considered, good performances can be achieved in terms of sedigraph simulations (NSE, RMSE and MAE all measure the adjustment between simulated and observed sedigraphs). This is because the calibration structure of the TETIS model allows compensating a lack in sediment availability (in this case, absence of initial deposits) with an increase of the sediment production coefficient. To confirm this statement, it can be seen that strategy 0 has the highest α coefficient value (see Table 2).

Despite the overall satisfactory performance of all strategies, some model limitations can be identified. For example, from Fig. 6 it can be seen that all strategies underestimate the peak discharge for Q01 in March 83 and 84. The model does not take into account phenomena like mass movements (e.g. landslides) or bank erosion, probably leading to the underestimation shown in Fig. 6. Another example of model error is the overestimation of the peak discharge at Q06 for the May 83 event. Nevertheless, taking into account possible model errors, parameter errors and the measurement precision, the results can be considered highly satisfactory.

Fig. 7 depicts the scatterplot of observed versus simulated fine sediment volume for each strategy. The results from five flood events and five stream gauge stations are shown. The median error is +2%, +16% and +5% for strategy 0, 1 and 2 respectively, and the volume error is included into the ±50% band respectively for the 48%, 44% and 44% of the cases. Strategy 1 slightly tends to overestimate the fine sediment volume, as the volume error is positive in 60% of cases, while for strategies 0 and 2 the percentage of positive volume errors is 52% and 56% respectively.

Figs. 6 and 7 and Table 4 show that all strategies provide satisfactory results in terms of fine sediment temporal discharge and total volume reproduction for almost all events and stream gauge stations. The model performance is quite similar for all strategies, and no systematic bias can be found for the strategies considered. Nevertheless, a deeper analysis is required in order to assess the model behaviour. For this reason, we carried out an exhaustive hysteresis loop analysis, which is shown as follows.

Table 4
Sediment sub-model calibration and validation results in terms of Nash and Sutcliffe Efficiency (NSE) for all strategies (the calibration events are highlighted in grey – August 1982 at stations Q01 and Q06). The best result for each event-station is shown in bold.

Event	Station	Strategy		
		0	1	2
Aug-1982	Q01	0.7678	**0.7860**	0.7848
	Q04	0.3145	**0.3610**	0.3482
	Q06	0.9126	0.9166	**0.9334**
	Q07	0.5241	**0.6375**	0.5030
	Q08	0.5407	0.6363	**0.8279**
Mar-1983	Q01	0.5059	0.4336	**0.6431**
	Q04	**0.6482**	0.0341	0.6346
	Q06	**0.7024**	−1.8177	−0.9917
	Q07	0.4729	−0.8129	**0.5715**
	Q08	0.3904	−0.1086	**0.5042**
May-1983	Q01	0.8849	0.9086	**0.9175**
	Q04	0.5441	0.5980	**0.8473**
	Q06	−1.8006	−1.9406	−1.1217
	Q07	0.5637	**0.5766**	0.3208
	Q08	**0.9040**	0.8905	0.8141
Nov-1983	Q01	0.5449	**0.6965**	0.5214
	Q04	**0.9302**	0.9157	0.9260
	Q06	−0.2701	0.0534	−1.0347
	Q07	**0.8981**	0.8620	0.8303
	Q08	**0.7167**	0.6850	0.6912
Mar-1984	Q01	0.5743	**0.7027**	0.5695
	Q04	0.6924	**0.7706**	0.5782
	Q06	**0.5844**	0.5264	0.5412
	Q07	0.2946	**0.4078**	0.1691
	Q08	0.2241	**0.3540**	0.2142

5.2. Hysteresis loop results

Fig. 8 presents the hysteresis loops observed in the water discharge – fine sediment discharge relationship. The results from two stream gauges, Q01 and Q06, are presented in this figure in order to analyse separately the effect of initial sediment condition in channels and gullies (Q06 sub-catchment has no river channel cells).

From Fig. 8, it can be seen that all strategies have different behaviours in terms of hysteresis loop. In the calibration event, August 1982, the best results are obtained with strategy 2, both at Q01 and Q06, although all simulated loops are rather thinner than the observed ones. For the March 1983 event, all models failed to simulate the hysteresis loop at Q01, due to a substantial underestimation of the fine sediment peak discharge (Fig. 7, Mar-83 event, Q01 sedigraph). At Q06 only the strategy 1 showed a hysteresis loop. Concerning the May 1983 event, strategies 1 and 2 showed acceptable hysteresis loops at Q01. At Q06, all strategies failed in replicating the hysteresis loop due to an overestimation of the observed fine sediment peak. Regarding November 1983 event, all strategies obtained a rather good reproduction of the hysteresis

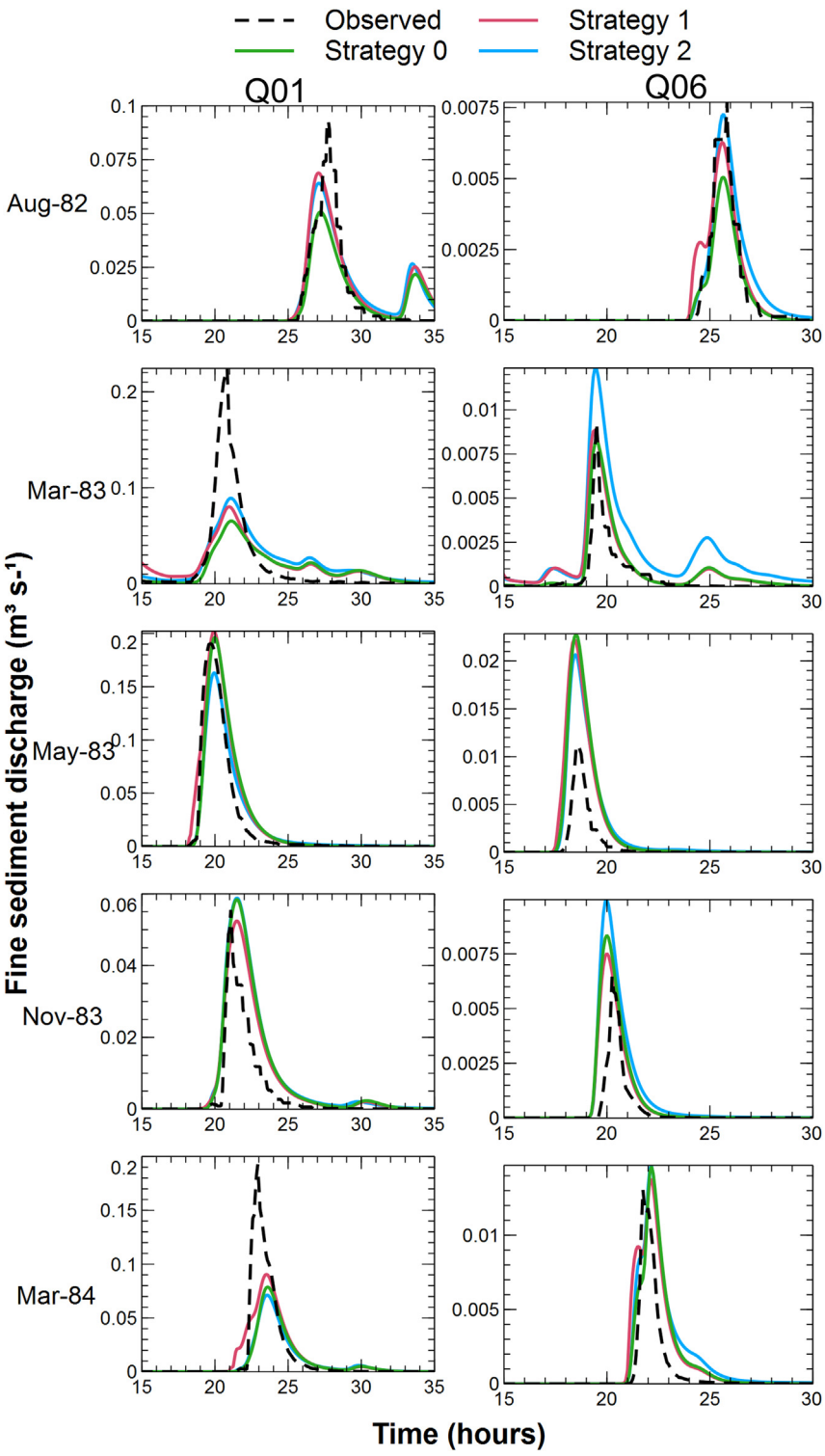

Fig. 6. Observed and simulated sedigraphs (fine sediment discharge) of all considered flood events at stations Q01 (left column) and station Q06 (right column).

loop at Q01, but only strategies 0 and 1 provided a loop at Q06. Lastly, for March 1984 event, none of the proposed strategies showed acceptable performances at Q01, although at Q06 the results of strategies 1 can be considered acceptable.

The shape of hysteresis loops was also analysed. Among the observed data of the available five events and five stream gauge stations, four types of loops were identified, following Nistor and Church (2005), as shown in Fig. 9: unique curve (no hysteresis loop), clockwise loop, counter clockwise loop and eight-shaped loop. The clockwise loop was the most frequent type (18 times out of 25), followed by counter clockwise loop (3), eight-shaped loop (3) and unique curve (1). A further type of curve was detected among the simulation results: the loop and unique curve. This last type denotes the development of a hysteresis loop (usually clockwise) which cannot be completed due to an early lack of available material.

Table 5
Sediment sub-model calibration and validation results in terms of Root Mean Square Error (RMSE) for all strategies (the calibration events are highlighted in grey – August 1982 at stations Q01 and Q06). The best result for each event-station is shown in bold.

Event	Station	Strategy		
		0	1	2
Aug-1982	Q01	0.0052	**0.0050**	**0.0050**
	Q04	0.0082	**0.0079**	0.0080
	Q06	**0.0002**	**0.0002**	**0.0002**
	Q07	0.0016	**0.0014**	0.0017
	Q08	0.0009	0.0008	**0.0005**
Mar-1983	Q01	0.0250	0.0267	**0.0212**
	Q04	**0.0024**	0.0040	**0.0024**
	Q06	**0.0005**	0.0015	0.0013
	Q07	0.0010	0.0019	**0.0009**
	Q08	0.0012	0.0016	**0.0010**
May-1983	Q01	0.01204	0.01073	**0.01020**
	Q04	0.00419	0.00393	**0.00242**
	Q06	0.00231	0.00236	**0.00201**
	Q07	0.00684	**0.00674**	0.00854
	Q08	**0.00083**	0.00089	0.00115
Nov-1983	Q01	0.00475	**0.00388**	0.00487
	Q04	**0.00055**	0.00061	0.00057
	Q06	0.00070	**0.00060**	0.00088
	Q07	**0.00038**	0.00044	0.00048
	Q08	**0.00050**	0.00053	0.00053
Mar-1984	Q01	0.01622	**0.01355**	0.01631
	Q04	0.00307	**0.00265**	0.00360
	Q06	**0.00091**	0.00097	0.00096
	Q07	0.00359	**0.00329**	0.00390
	Q08	0.00301	**0.00274**	0.00303

Strategy 0 provided 7 clockwise loops (out of 25 cases), 6 unique curves, 6 eight-shaped loops, 3 counter clockwise loops and 2 loop and unique curves. Strategy 1 provided a clear majority of clockwise loops (20), 2 loop and unique curves, one counter clockwise loop, one eight-shaped loop and one unique curve. Strategy 2 provided 9 counter clockwise loops, 8 clockwise loops, 5 unique curves 2 eight-shaped loops and one loop and unique curve. These results indicate that strategy 0 tends to show no loop (or a unique curve), as expected, given that sediment initial condition in gullies and channels is one of the main causes of hysteresis loop generation. On the other hand, strategy 1 tends to provide a clockwise loop in almost all cases. This can be considered a positive result, given that the observed data that also show clockwise loops are the most frequent type of water/sediment discharge relationship. Strategy 2 provides controversial results, as is capable to reproduce all types of loops, but tends to provide many counter clockwise loops which were not observed in the field measurements.

In order to evaluate all strategies from a loop reproduction point of view, the number of correct guesses (i.e. the number of times the model reproduce correctly the loop shape) was accounted for each strategy. Strategy 0 obtained the right loop shape 8 times, strategy 1 obtained the right loop shape 14 times and strategy 2 obtained the right loop shape 7 times (Table 7). Therefore, strategy 1 is clearly the most appropriate for hysteresis loop reproduction. Strategy 0 tends to show a unique curve, and for this reason is not adequate for loop simulation. An interesting example of this statement is May 1983 event at Q01 (strategy 0): both visual fit (Fig. 6) and NSE (Table 4) indicate a very good performance, but no hysteresis loop is simulated, while the observed data show a clockwise loop (Fig. 8). Strategy 2 looks, in some cases, also rather inadequate for loop reproduction, although it is the only strategy which appears capable of representing all loop types. For example is the only strategy capable to reproduce the counter clockwise loop in March 1984 event, Q06 station (Table 7).

In order to assess from a quantitative point of view the hysteresis loop simulation performance, the Hysteresis Index (HI_{mid}) presented by Lawler et al. (2006) was calculated for each event and each station. This index is based on measuring the 'fatness' of the loop at a given intermediate point between the maximum and the minimum water discharge – in this case at the 50% of the water discharge, as done by Lawler et al. (2006). This index is calculated by firstly determining the mid-point discharge given by:

$$Q_{w,\mathrm{mid}} = 0.5 \times (Q_{w,\max} - Q_{w,\min}) + Q_{w,\min} \quad \left(\mathrm{m^3\ s^{-1}}\right) \qquad (4)$$

Table 6
Sediment sub-model calibration and validation results in terms of Mean Absolute Error (MAE) for all strategies (the calibration events are highlighted in grey – August 1982 at stations Q01 and Q06). The best result for each event-station is shown in bold.

Event	Station	Strategy		
		0	1	2
Aug-1982	Q01	**0.001310**	0.001466	0.001638
	Q04	0.001149	**0.001108**	0.001152
	Q06	**0.000038**	0.000039	0.000054
	Q07	**0.000245**	0.000246	0.000265
	Q08	0.000121	0.000130	**0.000087**
Mar-1983	Q01	0.009528	0.014157	**0.009169**
	Q04	**0.000857**	0.002120	0.001265
	Q06	**0.000185**	0.000806	0.000685
	Q07	**0.000417**	0.001018	0.000510
	Q08	**0.000411**	0.000823	0.000536
May-1983	Q01	0.004114	0.003908	**0.003346**
	Q04	0.001133	0.001093	**0.000743**
	Q06	0.000579	0.000591	**0.000546**
	Q07	**0.001154**	0.001202	0.001578
	Q08	**0.000211**	0.000229	0.000243
Nov-1983	Q01	0.001634	**0.001391**	0.001729
	Q04	0.000129	**0.000125**	0.000140
	Q06	0.000125	**0.000104**	0.000182
	Q07	**0.000058**	0.000067	0.000086
	Q08	**0.000077**	0.000081	0.000086
Mar-1984	Q01	**0.003323**	0.003236	0.003420
	Q04	0.000563	**0.000507**	0.000678
	Q06	**0.000242**	0.000252	0.000322
	Q07	0.000564	**0.000533**	0.000616
	Q08	0.000436	**0.000412**	0.000437

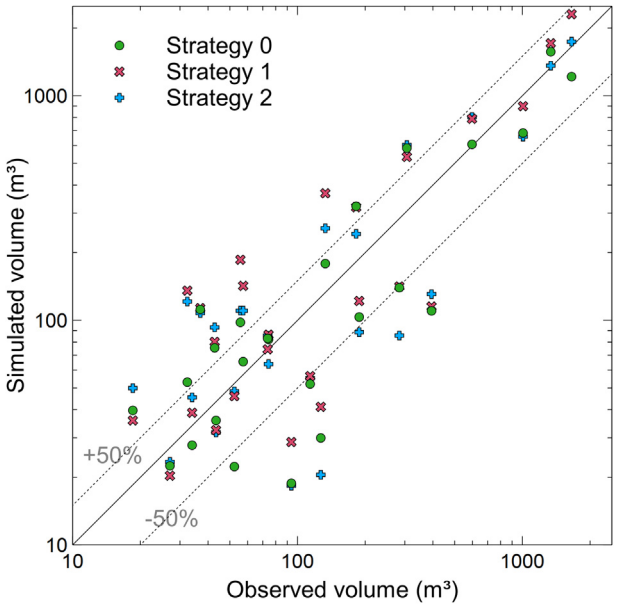

Fig. 7. Observed and simulated fine sediment volume for 5 event and 5 stream gauge stations, for all initial deposits estimation strategies.

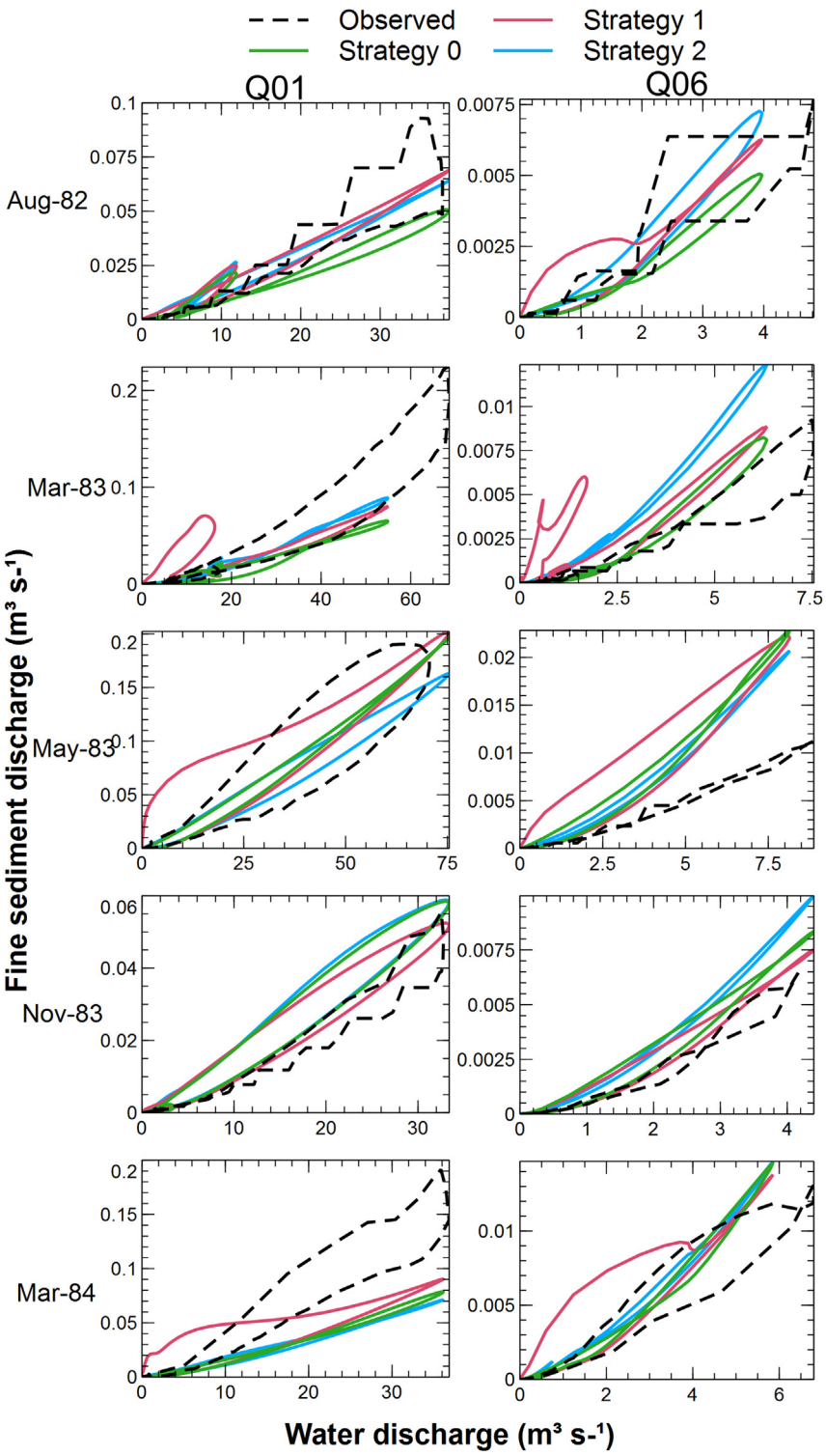

Fig. 8. Hysteresis loops (fine sediment discharge) of all considered flood events at stations Q01 (left column) and Q06 (right column).

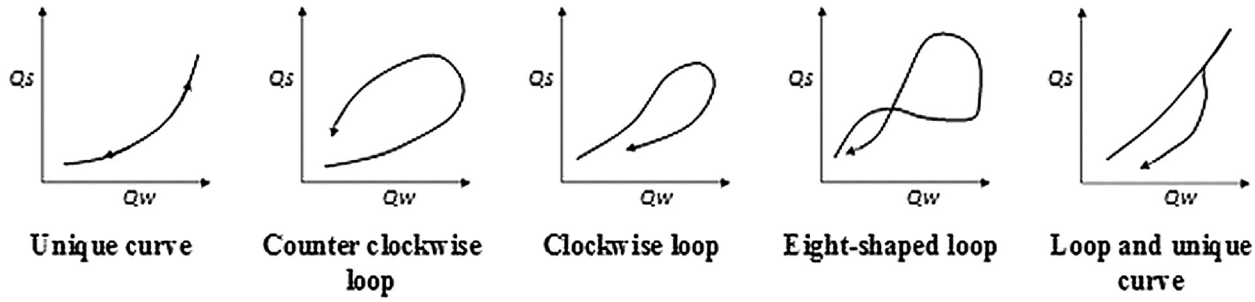

Fig. 9. Hysteresis loop types (modified from Nistor and Church, 2005). Q_s indicates sediment discharge and Q_w indicates water discharge.

where $Q_{w,\min}$ and $Q_{w,\max}$ are the minimum and maximum water discharge. Then, the two sediment discharge values corresponding to $Q_{w,\mathrm{mid}}$ in the water/sediment discharge plot ($Q_{s,\mathrm{RL}}$ and $Q_{s,\mathrm{FL}}$, sediment discharge corresponding to $Q_{w,\mathrm{mid}}$ on the rising limb and falling limb of the hydrograph, respectively) are computed, and $\mathrm{HI}_{\mathrm{mid}}$ is calculated as follows:

$$\text{If } Q_{s,\mathrm{RL}} > Q_{s,\mathrm{FL}} : \mathrm{HI}_{\mathrm{mid}} = Q_{s,\mathrm{RL}}/Q_{s,\mathrm{FL}} - 1 \quad (-) \tag{5}$$

$$\text{If } Q_{s,\mathrm{RL}} < Q_{s,\mathrm{FL}} : \mathrm{HI}_{\mathrm{mid}} = -1/(Q_{s,\mathrm{RL}}/Q_{s,\mathrm{FL}}) + 1 \quad (-) \tag{6}$$

The interpretation of this index is very simple: the greater the hysteresis, the greater $\mathrm{HI}_{\mathrm{mid}}$. This index can also distinguish between clockwise and counter clockwise loops, depending on the sign of its value (positive for clockwise and negative for counter clockwise), although it does not recognise eight-shaped and unique loops.

This index was computed for the 25 observed loops and for the 25 × 3 simulated loops. The results are shown in Fig. 10.

Nineteen of observed loops showed a positive index value while the other six loops a negative value. As can be seen in Fig. 10, the model behaviour is acceptable for positive values. In particular, strategy 1, as previously noticed with a visual loop analysis, provided the best behaviour in reproducing clockwise hysteresis, as it obtained the best model performance in 12 cases out of the 19 positive values. On the other hand, the model is often failing in reproducing negative values, given the high number of points in the up-left quadrant. Only strategy 2 can reproduce some negative value, although only when $\mathrm{HI}_{\mathrm{mid}}$ is close to zero.

Finally, in order to evaluate the error between observed and simulated loops, a similarity index was also calculated for each event and each stream gauge, representing the mean Cartesian distance between the observed and the simulated water discharge – sediment discharge points (Eq. (7)).

$$I = \frac{1}{n}\sum_{i=1}^{n}\sqrt{\left(Q_{w,i} - \widehat{Q}_{w,i}\right)^2 + \left(Q_{s,i} - \widehat{Q}_{s,i}\right)^2} \quad (-) \tag{7}$$

where I is the loop similarity index, n is the number of time steps, $Q_{w,i}$ is the observed water discharge, $\widehat{Q}_{w,i}$ is the simulated water discharge, $Q_{s,i}$ is the observed fine sediment discharge, $\widehat{Q}_{w,i}$ is the simulated fine sediment discharge. This index provides a similarity indicator between observed and simulated hysteresis loop. The median value of all 25 calculated indexes (resulting from 5 events and 5 stream gauge stations) were respectively 0.124450, 0.124449 and 0.124444. The best median index value was provided by strategy 2. Nevertheless, it was found that, among 25 hysteresis loops, strategy 0 obtained the best performance eight times, strategy 1 twelve times and strategy 2 five times. This analysis also confirms the previous stated conclusions. Strategy 1 is the most adequate strategy for loop reproduction, because it obtains the maximum number of best fitting index values, although strategy 2 obtained the lowest index median value, which indicates also a

Table 7
Hysteresis loop shape analysis (loop types are shown in Fig. 9).

		Observed loop	Strategy 0	Strategy 1	Strategy 2
Aug-1982	Q01	Counter clockwise	Counter clockwise	Clockwise	Clockwise
	Q04	Clockwise	Unique curve	Clockwise	Eight-shaped
	Q06	Clockwise	Eight-shaped	Loop-unique	Counter clockwise
	Q07	Clockwise	Loop-unique	Clockwise	Counter clockwise
	Q08	Eight-shaped	Eight-shaped	Clockwise	Counter clockwise
Mar-83	Q01	Clockwise	Counter clockwise	Clockwise	Unique curve
	Q04	Clockwise	Unique curve	Clockwise	Clockwise
	Q06	Clockwise	Counter clockwise	Clockwise	Unique curve
	Q07	Clockwise	Unique curve	Clockwise	Counter clockwise
	Q08	Clockwise	Clockwise	Counter clockwise	Counter clockwise
May-83	Q01	Clockwise	Unique curve	Clockwise	Clockwise
	Q04	Clockwise	Clockwise	Clockwise	Clockwise
	Q06	Counter clockwise	Loop-unique	Clockwise	Unique curve
	Q07	Clockwise	Clockwise	Clockwise	Counter clockwise
	Q08	Unique curve	Eight-shaped	Clockwise	Counter clockwise
Nov-83	Q01	Clockwise	Clockwise	Clockwise	Clockwise
	Q04	Clockwise	Clockwise	Clockwise	Clockwise
	Q06	Eight-shaped	Loop-unique	Clockwise	Unique curve
	Q07	Clockwise	Unique curve	Unique curve	Clockwise
	Q08	Clockwise	Eight-shaped	Eight-shaped	Eight-shaped
Mar-84	Q01	Clockwise	Eight-shaped	Clockwise	Loop-unique
	Q04	Eight-shaped	Clockwise	Clockwise	Clockwise
	Q06	Counter clockwise	Eight-shaped	Loop-unique	Counter clockwise
	Q07	Clockwise	Clockwise	Clockwise	Unique curve
	Q08	Clockwise	Unique curve	Clockwise	Counter clockwise

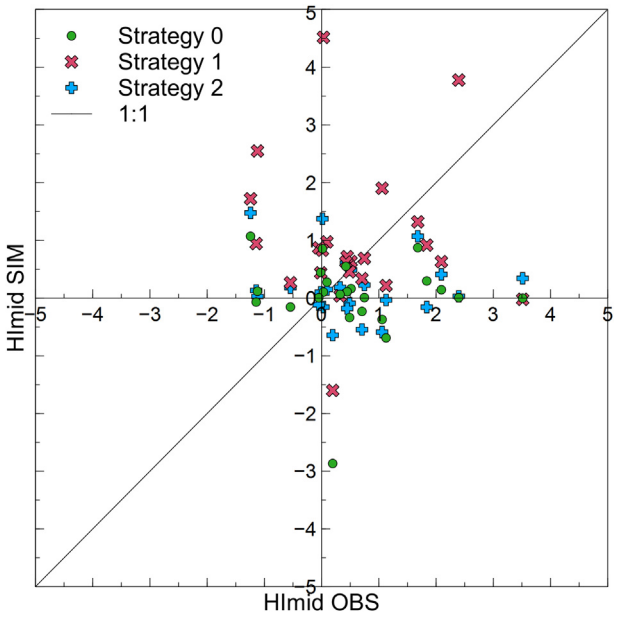

Fig. 10. Observed vs simulated Hysteresis Index (HI_{mid}) for all strategies.

rather positive performance. These results also show that, although model performances were highly satisfactory in terms of NSE or sedigraph reproduction, the model sometimes fails in adequately simulating the sediment-rating curve, no matter what strategy is used.

6. Summary and conclusions

The importance of initial sediment conditions on model calibration and validation is analysed using the model TETIS. The model was used to assess the effect of initial sediment condition (sediment texture and volume deposited in the drainage network at the beginning of a model run) on model calibration and validation. An automatic calibration module, based on the SCE-UA optimisation algorithm and an initial sediment condition setting tool were integrated into TETIS. The sediment sub-model calibration structure was also modified in order to allow a more flexible model calibration. The application was carried out on the experimental catchment of Goodwin Creek (US).

Three strategies for initial sediment condition estimation were considered: strategy 0 – no sediment availability within the drainage network; strategy 1 – calibration of the available sediment volume within the drainage network; and strategy 2 – estimation of sediment initial condition using a warm-up simulation.

The three models were automatically calibrated by adjusting the hillslope, gully and channel sediment transport capacity in order to reproduce the observed fine sedigraph of single storm events. The models were then validated considering four additional events.

The resulting calibration parameter sets showed that employing initial sediment deposits estimation strategy strongly affects model calibration and behaviour. The results of the calibration and validation processes at the event-scale show a strong dependence of model results (both in terms of simulated sediment discharge and simulated hysteresis loop) on the initial conditions of the deposited sediment. Therefore, an adequate estimation of the loose deposited sediments at the beginning of the storm event is fundamental for a proper event scale modelling of soil erosion and sediment transport of the Goodwin Creek catchment.

The comparison between observed and simulated sedigraphs showed that all strategies provided adequate results. The model provided a satisfactory performance in terms of NSE, RMSE, MAE and volume error (median NSE = 0.564, 0.598 and 0.572 for strategy 0, 1 and 2 respectively). From an analysis of the sedigraph, none of the proposed strategies provided significantly better results than the other two, although strategies 1 and 2 appeared to be more reliable than strategy 0, as expected.

The loop rating curve analysis demonstrated that the choice of initial sediment conditions affected the simulation results. The qualitative and quantitative hysteresis loop analysis showed that, despite the good model performance, the model was sometimes not able to reproduce the catchment erosion and deposition dynamic, as various loops were not correctly simulated. This proved that a good sedigraph validation may not be sufficient to prove the sediment model reliability.

Without any initial sediment condition, the model results were typically inferior to the results with initial condition manual calibration or warm-up simulation. Strategy 1 clearly showed the best results in term of clockwise loop reproduction, although it failed in simulating other loop types. Strategy 2 showed the best results in terms of reproducing different loop shapes, although in many cases it also failed in reproducing the correct hysteresis loop type.

Acknowledgements

This study was supported by the Spanish Ministry of Economy and Competitiveness through the research projects FLOOD-MED (CGL2 008-06474-C02-02/BTE), Consolider-SCARCE (CSD2009-00065) and ECOTETIS (CGL2011-28776-C02-01).

References

Aksoy, H., Kavvas, M.L., 2005. A review of hillslope and watershed scale erosion and sediment transport models. Catena 64 (2–3), 247–271. http://dx.doi.org/10.1016/j.catena.2005.08.008.

Alonso, C.V., 1996. Hydrologic research on the USDA Goodwin Creek experimental watershed, northern Mississippi. In: Proc. 16th Annual AGU Hydrology Days Conf, pp. 25–36.

Andrés-Doménech, I., Múnera, J.C., Francés, F., Marco, J.B., 2010. Coupling urban event-based and catchment continuous modelling for combined sewer overflow river impact assessment. Hydrol. Earth Sys. Sci. 14, 2057–2072 http://dx.doi.org/10.5194/hess-14-2057-2010.

Bennett, N.D., Croke, B.F.W., Guariso, G., Guillaume, J.H.A., Hamilton, S.H., Jakeman, A.J., Marsili-Libelli, S., Newham, L.T.H., Norton, J.P., Perrin, C., Pierce, S.A., Robson, B., Seppelt, R., Voinov, A.A., Fath, B.D., Andreassian, V., 2013. Characterising performance of environmental models. Environ. Modell. Softw. 40, 1–20 http://dx.doi.org/10.1016/j.envsoft.2012.09.011.

Beven, K., 1989. Changing ideas in hydrology: the case of physically-based models. J. Hydrol. 105 (1), 157–172 http://dx.doi.org/10.1016/0022-1694(89)90101-7.

Blackmarr, W.A., 1995. Documentation of Hydrologic, Geomorphic, and Sediment Transport Measurements on the Goodwin Creek Experimental Watershed, Northern Mississippi, for the Period 1982-1993, Preliminary Release. US Department of Agriculture, National Sedimentation Laboratory, Oxford, MS, 41 p.

Boiten, W., 2003. Hydrometry. Taylor & Francis, 256 p.

Brath, A., Montanari, A., Toth, E., 2004. Analysis of the effects of different scenarios of historical data availability on the calibration of a spatially-distributed hydrological model. J. Hydrol. 291 (3–4), 232–253 http://dx.doi.org/10.1016/j.jhydrol.2003.12.044.

Bussi, G., Rodríguez-Lloveras, X., Francés, F., Benito, G., Sánchez-Moya, Y., Sopeña, A., 2013. Sediment yield model implementation based on check dam infill stratigraphy in a semiarid Mediterranean catchment. Hydrol. Earth Sys. Sci. 10 (3), 3427–3466 http://dx.doi.org/10.5194/hess-17-3339-2013.

de Roo, A., Jetten, V., 1999. Calibrating and validating the LISEM model for two data sets from the Netherlands and South Africa. Catena 37 (3–4), 477–493. http://dx.doi.org/10.1016/S0341-8162(99)00034-X.

de Roo, A., Wesseling, C.G., Ritsema, C.J., 1996. LISEM: a single-event physically based hydrological and soil erosion model for drainage basins. I: theory, input and output. Hydrol. Process 10 (8), 1107–1117. http://dx.doi.org/10.1002/(SICI)1099-1085(199608)10:8<1107::AID-HYP415>3.0.CO;2-4.

de Vente, J., Poesen, J., Bazzoffi, P., Vand Rompaey, A., Goverts, G., 2008. Spatially distributed modelling of soil erosion and sediment yield at regional scales in Spain. Glob. Planet Change 60, 147–168. http://dx.doi.org/10.1016/j.gloplacha.2007.05.002.

Duan, Q., Sorooshian, S., Gupta, V., 1992. Effective and efficient global optimization for conceptual rainfall-runoff models. Water Resour. Res. 28 (4), 1015–1031 http://dx.doi.org/10.1029/91WR02985.

Duan, Q., Sorooshian, S., Gupta, V., 1994. Optimal use of the SCE-UA global optimization method for calibrating watershed models. J. Hydrol. 158 (3), 265–284 http://dx.doi.org/10.1016/0022-1694(94)90057-4.

Eder, A., Strauss, P., Krueger, T., Quinton, J.N., 2010. Comparative calculation of suspended sediment loads with respect to hysteresis effects (in the Petzenkirchen catchment, Austria). J. Hydrol. 389 (1–2), 168–176 http://dx.doi.org/10.1016/j.jhydrol.2010.05.043.

Engelund, F., Hansen, E., 1967. A Monograph on Sediment Transport in Alluvial Streams. Monogr, Denmark Tech Univ, Hydraul Lab, 62 p.

England Jr., J., Velleux, M., Julien, P.Y., 2007. Two-dimensional simulations of extreme floods on a large watershed. J. Hydrol. 347 (1), 229–241 http://dx.doi.org/10.1016/j.jhydrol.2007.09.034.

Favis-Mortlock, D., Boardman, J., MacMillan, V., 2001. The limits of erosion modeling: why we should proceed with care. In: Harmon, R.S., Doe, W.W. (Eds.), Landscape Erosion and Evolution Modeling. Kluwer Academic Publishers, New York, pp. 477–516.

Folly, A., Quinton, J.N., Smith, R.E., 1999. Evaluation of the EUROSEM model using data from the Catsop watershed, The Netherlands. Catena 37 (3), 507–519. http://dx.doi.org/10.1016/S0341-8162(99)00036-3.

Francés, F., Vélez, J.J., Vélez, J.I., Puricelli, M., 2002. Distributed modelling of large basins for a real time flood forecasting system in Spain. In: Proceedings Second Federal Interagency Hydrologic Modelling Conference. Las Vegas, USA. July, pp. 3513–3524. CD Format. Gan, TY and Biftu, GF.

Francés, F., Vélez, J.I., Vélez, J.J., 2007. Split-parameter structure for the automatic calibration of distributed hydrological models. J. Hydrol. 332 (1), 226–240 http://dx.doi.org/10.1016/j.jhydrol.2006.06.032.

Francés, F., García-Bartual, R., Bussi, G., 2011. High return period annual maximum reservoir water level quantiles estimation using synthetic generated flood events. In: Risk Analysis, Dam Safety, Dam Security and Critical Infrastructure Management. Taylor & Francis Group, London, pp. 185–190.

Freedman, V.L., Lopes, V.L., Hernandez, M., 1998. Parameter identifiability for catchment-scale erosion modelling: a comparison of optimization algorithms. J. Hydrol. 207, 83–97 http://dx.doi.org/10.1016/S0022-1694(98)00131-0.

Harmon, R.S., Doe III, W.W. (Eds.), 2001. Landscape Erosion and Evolution Modelling. Kluwer Academic, New York, 540 pp.

Jetten, V., de Roo, A., Favis-Mortlock, D., 1999. Evaluation of field-scale and catchment-scale soil erosion models. Catena 37 (3–4), 521–541. http://dx.doi.org/10.1016/S0341-8162(99)00037-5.

Johnson, B.E., Julien, P.Y., Molnar, D.K., Watson, C.C., 2000. The Two-dimensional Upland Erosion Model CASC2D-SED. IAHS Publication, pp. 107–126. http://dx.doi.org/10.1111/j.1752-1688.2000.tb04246.x.

Julien, P., 2002. River Mechanics. Cambridge University Press, 434 pp.

Julien, P.Y., Rojas, R., 2002. Upland erosion modeling with CASC2D-SED. Int. J. Sediment. Res. 17 (4), 265–274.

Julien, P., 2010a. Erosion and Sedimentation, second ed. Cambridge University Press. 280 pp.

Julien, P.Y., 2010b. Erosion and Sedimentation, second ed. Cambridge University Press. 371 p.

Karydas, C.G., Panagos, P., Gitas, I.Z., 2012. A classification of water erosion models according to their geospatial characteristics. Int. J. Digital Earth, 1–22. http://dx.doi.org/10.1080/17538947.2012.671380.

Kilinc, M., Richardson, E.V., 1973. Mechanics of Soil Erosion from Overland Flow Generated by Simulated Rainfall. Colorado State University. Hydrology Papers.

Klemeš, V., 1986. Operational testing of hydrological simulation models. Hydrol. Sci. J. 31 (1), 13–24 http://dx.doi.org/10.1080/02626668609491024.

Kuhnle, R.A., Willis, J.C., Bowie, A.J., 1989. Total sediment load calculations for Goodwin Creek. In: Wang, S. (Ed.), Sediment Transport Modeling. Proceedings of the International Symposium, pp. 700–705. New Orleans.

Kuhnle, R.A., Bingner, R.L., Foster, G.R., Grissinger, E.H., 1996. Effect of land use changes on sediment transport in Goodwin Creek. Water Resour. Res. 32 (10), 3189–3196 http://dx.doi.org/10.1029/96WR02104.

Kuhnle, R.A., Bingner, R.L., Langendoen, E.J., Simon, A., Wilson, C.G., Shields Jr., F.D., ARS USDA, 2005. Goodwin Creek Experimental Watershed – Assessment of Conservation and Environmental Effects, 2005 ASAE Annual International Meeting.

Lawler, D.M., Petts, G.E., Foster, I.D.L., Harper, S., 2006. Turbidity dynamics during spring storm events in an urban headwater river system: the Upper Tame, West Midlands, UK. Sci. Tot Environ. 360 (1–3), 109–126 http://dx.doi.org/10.1016/j.scitotenv.2005.08.032.

Merritt, W.S., Letcher, R.A., Jakeman, A.J., 2003. A review of erosion and sediment transport models. Environ. Modell. Softw. 18 (8), 761–799 http://dx.doi.org/10.1016/S1364-8152(03)00078-1.

Molnár, P., Ramírez, J.A., 1998. An analysis of energy expenditure in Goodwin Creek. Water Resour. Res. 34 (7), 1819–1829.

Morgan, R.P.C., Quinton, J.N., Smith, R.E., Govers, G., Poesen, J.W.A., Auerswald, K., Chisci, G., Torri, D., Styczen, M.E., 1998. The European Soil Erosion Model (EUROSEM): a dynamic approach for predicting sediment transport from fields and small catchments. Earth Surf. Proc. Land. 23 (6), 527–544 http://dx.doi.org/10.1002/(SICI)1096-9837(199806)23:6%3C527::AID-ESP868%3E3.0.CO;2-5.

Moriasi, D.N., Arnold, J.G., Van Liew, M.W., Bingner, R.L., Harmel, R.D., Veith, T.L., 2007. Model evaluation guidelines for systematic quantification of accuracy in watershed simulations. Trans. ASABE 50 (3), 885–900.

Nash, J.E., Sutcliffe, J.V., 1970. River flow forecasting through conceptual models – part 1-A discussion of principles. J. Hydrol. 10 (3), 282–290 http://dx.doi.org/10.1016/0022-1694(70)90255-6.

Newham, L.T.H., Letcher, R.A., Jakeman, A.J., Kobayashi, T., 2004. A framework for integrated hydrologic, sediment and nutrient export modelling for catchment-scale management. Environ. Modell. Softw. 19 (11), 1029–1038 http://dx.doi.org/10.1016/j.envsoft.2003.11.006.

Nistor, C.J., Church, M., 2005. Suspended sediment transport regime in a debris-flow gully on Vancouver Island. Hydrol. Process 19 (4), 861–885. http://dx.doi.org/10.1002/hyp.5549.

Ogden, F.L., Heilig, A., 2001. Two-dimensional watershed-scale erosion modeling with CASC2D. In: Harmon, R.S., Doe, W.W. (Eds.), Landscape Erosion and Evolution Modeling. Kluwer Academic Publishers, New York, pp. 277–316.

Oreskes, N., Shrader-Frechette, K., Belitz, K., 1994. Verification, validation, and confirmation of numerical models in the earth sciences. Science 263, 641–646. http://dx.doi.org/10.1126/science.263.5147.641.

Osterkamp, W.R., Toy, T.J., 1997. Geomorphic considerations for erosion prediction. Environ. Geol. 29, 152–157 http://dx.doi.org/10.1007/s002540050113.

Owens, P.N., Collins, A.J., 2006. Soil Erosion and Sediment Redistribution in River Catchments: Measurement, Modelling and Management. CABI.

Piest, R.F., Bradford, J.M., Wyatt, G.M., 1975. Soil erosion and sediment transport from gullies. J. Hydraul. Div. 101 (1), 65–80.

Polyakov, V., Fares, A., Kubo, D., Jacobi, J., Smith, C., 2007. Evaluation of a non-point source pollution model, AnnAGNPS, in a tropical watershed. Environ. Modell. Softw. 22 (11), 1617–1627 http://dx.doi.org/10.1016/j.envsoft.2006.12.001.

Rojas, R., 2002. GIS-based Upland Erosion Modeling, Geovisualization and Grid Size Effects on Erosion Simulations with CASC2D-SED (PhD dissertation). Colorado State University, 325 p.

Salazar, S., Francés, F., Komma, J., Blume, T., Francke, T., Bronstert, A., Blöschl, G., 2013. A comparative analysis of the effectiveness of flood management measures based on the concept of "retaining water in the landscape" in different European hydro-climatic regions. Nat. Hazards Earth Syst. Sci. 12 (11), 3287–3306 http://dx.doi.org/10.5194/nhess-12-3287-2012.

Santos, C.A.G., Srinivasan, V.S., Suzuki, K., Watanabe, M., 2003. Application of an optimization technique to a physically based erosion model. Hydrol. Process 17, 989–1003. http://dx.doi.org/10.1002/hyp.1176.

Santos, C.A.G., Maia Pinto, L.E., Machado Freire, P.K., Mishra, S.K., 2010. Application of a particle swarm optimization to a physically-based erosion model. Ann. Warsaw Univ. Life Sci. – SGGW 42 (1), 39–49. http://dx.doi.org/10.2478/v10060-008-0063-9.

Saxton, K.E., Rawls, W.J., 2006. Soil water characteristic estimates by texture and organic matter for hydrologic solutions. Soil. Sci. Soc. Am. J. 70, 1569–1578 http://dx.doi.org/10.2136/sssaj2005.0117.

Seeger, M., Errea, M.P., Beguería, S., Arnáez, J., Martí, C., García-Ruiz, J.M., 2004. Catchment soil moisture and rainfall characteristics as determinant factors for discharge/suspended sediment hysteretic loops in a small headwater catchment in the Spanish Pyrenees. J. Hydrol. 288 (3), 299–311 http://dx.doi.org/10.1016/j.jhydrol.2003.10.012.

Senarath, S.U.S., Ogden, F.L., Downer, C.W., Sharif, H.O., 2000. On the calibration and verification of two-dimensional, distributed, Hortonian, continuous watershed models. Water Resour. Res. 36 (6), 1495–1510 http://dx.doi.org/10.1029/2000WR900039.

Smith, H.G., Dragovich, D., 2009. Interpreting sediment delivery processes using suspended sediment-discharge hysteresis patterns from nested upland catchments, south-eastern Australia. Hydrol. Process 23 (17), 2415–2426. http://dx.doi.org/10.1002/hyp.7357.

Vanmaercke, M., Maetens, W., Poesen, J., Jankauskas, B., Jankauskiene, G., Verstraeten, G., de Vente, J., 2012. A comparison of measured catchment sediment yields with measured and predicted hillslope erosion rates in Europe. J. Soils Sediments, 1–17. http://dx.doi.org/10.1007/s11368-012-0479-z.

Van Oost, K., Govers, G., Cerdan, O., Thauré, D., Van Rompaey, A., Steegen, A., Nachtergaele, J., Takken, I., Poesen, J., 2005. Spatially distributed data for erosion model calibration and validation: the Ganspoel and Kinderveld datasets. Geomorphology 65 (1), 157–169. http://dx.doi.org/10.1016/j.catena.2005.03.001.

Van Rompaey, A., Bazzoffi, P., Jones, R.J.A., Montanarella, L., 2005. Modeling sediment yields in Italian catchments. Geomorphology 65 (1), 157–169. http://dx.doi.org/10.1016/j.geomorph.2004.08.006.

Vélez, J.J., Puricelli, M., López Unzu, F., Francés, F., 2009. Parameter extrapolation to ungauged basins with a hydrological distributed model in a regional framework. Hydrol. Earth Sys. Sci. 13 (2), 229–246 http://dx.doi.org/10.5194/hess-13-229-2009.

Velleux, M., Julien, P.Y., Rojas, R., Clements, W., England Jr., J., 2006. Simulation of metals transport and toxicity at a mine-impacted watershed: California Gulch, Colorado. Environ. Sci. Technol. 40 (22), 6996–7004.

Verstraeten, G., 2006. Regional scale modelling of hillslope sediment delivery with SRTM elevation data. Geomorphology 81 (1), 128–140. http://dx.doi.org/10.1016/j.geomorph.2006.04.005.

Viney, N.R., Sivapalan, M., 1999. A conceptual model of sediment transport: application to the Avon River Basin in Western Australia. Hydrol. Process 13 (5), 727–743. http://dx.doi.org/10.1002/(SICI)1099-1085(19990415)13:5<727::AID-HYP776>3.0.CO;2-D.

Wicks, J.M., Bathurst, J.C., 1996. SHESED: a physically based, distributed erosion and sediment yield component for the SHE hydrological modelling system. J. Hydrol. 175 (1–4), 213–238 http://dx.doi.org/10.1016/S0022-1694(96)80012-6.

Williams, G.P., 1989. Sediment concentration versus water discharge during single hydrologic events in rivers. J. Hydrol. 111 (1), 89–106 http://dx.doi.org/10.1016/0022-1694(89)90254-0.